Bi-Elliptic Transfer and Stability Analysis of Lagrange Points

Yutian Sebastian Chen

Received February 24, 2025
Accepted June 12, 2025
Electronic access June 30, 2025

This paper reviews the science behind orbital mechanics and acts as a summary to the most commonly used orbital maneuvers. The analysis details Hohmann transfer orbits and bi-elliptic transfers, elucidating the conditions under which the latter may prove more efficient. Furthermore, we explore Lagrange points and their stability within the context of the restricted three-body problem of the Earth-Moon system. Lagrange points are analysed for their stability. Through the implementation of calculations in MATLAB, we visualise the trajectories of spacecraft engaged in orbital transfer and those around Lagrange points, corresponding positions at specific times. A case study on the orbital transfer period shows a synodic period of 780 days, the next optimal launch date in November of 2025. Throughout the paper, perturbations of relatively minor degree may not be taken into account. Finally, we introduce future research opportunities in optimizing transfer strategies to enhance energy conversion during maneuvers involving complex three-body systems.

Introduction

With the advancement of space technology, our understanding of orbital mechanics and its applications has evolved over time. The long-term dynamics of systems of bodies, including satellites, poses a significant unsolved problem. Orbital behaviors are based on Newtonian motion and Einsteins explanation of gravity[1], strongly supported by Keplers three laws. The history of orbital sciences begins with Nicolaus Copernicus (1473-1543), who first established the heliocentric model, where he places the sun in the center of the solar system).[2] Later Kepler derived his three laws to describe the elliptical orbits of bodies around the sun in his book "Harmonices Mundi"(Harmonics of the World).[3] Euler further advanced his theories based on Newton and Keplers work, formulating the equations of motion for rigid bodies, which are crucial in understanding the dynamics of rotating systems. With the introduction of general relativity, a slightly altered model of gravity was developed. This study is based off of such formulated models.

We now use these equations of orbital dynamics to carry out maneuvers, mostly using stellar observations or other satellite technology. Since the mid 20th century, there has also been a spur of crewed space missions. Currently, orbital analysis and determining trajectories of objects to a more detailed extent are the main areas of focus. The orbital determination methods and maneuvers are essential for the success of any kind of space mission, involving orbital rendezvous, cross-system orbital transfer, amongst other things.

Specific orbital positions, orbiting altitude, and spacecraft velocity are chosen for interplanetary trajectories, used for both manned and unmanned missions. Space agencies over the world have conducted extensive research on orbital transfers for the success of the Apollo missions, communication satellites, and much more. One of the notable missions is the GEM (Galileo Europa Mission). The GEM team details the mathematics involved in calculating flyby statistics that ensure that the spacecraft gathers data yet its orbit does not decay too much, to the point where it succumbs to Jupiters gravity[4].

In recent launches, JWST orbits L2. This choice was specific because it meant that it always faced away from the Earth-Sun system, staying in relative stability and free from major orbital perturbations. Minimal fuel is required to remain in orbit around L2 because of the characteristics of Lagrange points. Orbital transfers are also used in the docking of spacecraft with the ISS. Using direct docking maneuvers, the fuel requirements will be significantly higher than when slowing down the spacecraft and decreasing orbital radius, so the spacecraft speeds up relative to the ISS. The specific energy equation:

$$E = \frac{-\mu}{2r} \tag{1}$$

along with energy conservation show that if the radius of initial orbit is greater than the final orbit, then lowering the periapsis (furthest point) of the orbit will be the purpose of the required impulse. Here, E is the total specific energy of an object, μ is the standard gravitational parameter, and r is the semi-major axis of the orbiting body.

The Hohmann transfer maneuver, discovered by the German engineer Walter Hohmann showed the most economical trail between two celestial bodies.[5] It includes two burns, one to enter the transfer orbit, and one to circularize to the final orbit. Bi-elliptic transfers further focus on three-impulse orbital maneuver, where an intermediate elliptical orbit is chosen. The first burn occurs at periapsis (in the lower orbit) to increase velocity. This burn creates an elliptical orbit, with the apoapsis far beyond the target higher orbit. A second burn raises the periapsis of the new orbit to the desired higher orbit. The last burn circularizes the final orbit.

During missions, the priority is on most occasions fuel efficiency. Thus, most orbital transfers are centered around paths that utilize natural elements such as the slingshot effect, along with a mix of the two transfer mechanisms. The bi-elliptic Hohmann transfer will be more efficient when the total v required for the three impulses is less than the total v that the regular Hohmann transfer requires[6]. When the radii ratio reaches 11.94, the bi-elliptic transfers efficiency overcomes that of the faster Hohmann transfer. However, specific perturbations from any massive body out of the system can have significant impact on the choice of orbital maneuvers.

Exceptionally notable points in any system are the set of five points in space around the center of a system, where bodies can be balanced and kept in relative stability. These are known as the Lagrange points, discovered by Joseph-Louis Lagrange in 1772, using the restricted three-body problem.[7] The problem details the behavior of a non-massive object in the presence of two supermassive ones. Positions like the Lagrange Points balance the gravitational forces acting on said point. His work set the scene to stable, fuel-efficient movement of probes in the solar system. These points are used in astronomical observations to minimize interference, such as in JWST, which is further analysed in this study. The stability of Lagrange points varies: L4 and L5 are generally stable, while L1, L2, and L3 are unstable. In 1968, the physicist R. W. Farquhar discovered a fuel-efficient HALO orbit around L2, one that essentially wraps L2 and is useful for observations.[8] The stability analysis involves linearizing the equations of motion around these points and examining the eigenvalues of the resulting system. The intricate balancing can be further disturbed easily, requiring real-time precise maneuvering.

In this paper we derive the laws of motion, and orbital simulation has been carried out using the programming platform MATLAB. This study investigates bi-elliptic transfer and the Hohmann transfer maneuvers between two circular orbits in the Earths gravitational field, and the Suns gravitational field, as well as the stability analysis of Lagrange points. Further graphing shows the specific energy requirements to transfer to various points in the solar system, including when a threshold is reached and a spacecraft falls entirely into the gravitational pull of one of the planets.

Background and Methods

In the calculation of orbital transfers, the following assumptions are made:

- The Earth is considered a point mass, and its gravitational field is modeled using the standard gravitational parameter, $\mu = 3.986 \times 10^5 km^3/s^2$
- Perturbations due to atmospheric drag, solar radiation pressure, Earth oblateness, and gravitational influences from other celestial bodies are neglected in this section.
- Orbital transfers are assumed coplanar, with circular starting and ending trajectory.
- The spacecraft is treated as a point mass, and its propulsion system provides instantaneous velocity changes (impulsive changes).
- General Relativity is not considered in the local system of this paper

The assumptions will not create any major offsets, but given long-term effect, might make the results inaccurate. Accounting for the low-speed spacecrafts and lack of supermassive celestial bodies, relativistic corrections will not be of great impact to this studys results as well. This study will delve into the mathematical laws that govern orbital mechanics, further proving and investigating the topics mentioned above, focusing on coplanar orbital maneuvers. These conclusions is put into code inside the MATLAB software using the ODE 133[9] solver for better energy-conserving integration, graphing the results. Five evenly-spaced points were taken from the model and tested for energy cinservation, as available in the tables below.

Table 1 Energy conservation check for Hohmann transfer simulation

Hohmann Transfer	**Radius r (m)**	**Speed v (m/s)**	**KE (J/kg)**	**PE (J/kg)**	**Total E (J/kg)**
Point 1	1.50e+11	34,407.45	5.92e+08	-8.87e+08	-2.95e+08
Point 2	1.87e+11	28,766.48	4.14e+08	-7.09e+08	-2.95e+08
Point 3	2.25E+11	24,297.28	2.95e+08	-5.90e+08	-2.95e+08
Point 4	2.62e+11	20,522.42	2.11e+08	-5.06e+08	-2.95e+08
Point 5	3.00e+11	17,157.85	1.47e+08	-4.42e+08	-2.95e+08

Table 2 Energy Conservation check for Bi-elliptic transfer simulation

Bi-elliptic Transfer	**Radius r (m)**	**Speed v (m/s)**	**KE (J/kg)**	**PE (J/kg)**	**Total E (J/kg)**
Point 1	1.50e+11	37,684.77	7.10e+08	-8.87e+08	-1.77e+08
Point 2	1.87e+11	32,615.63	5.32e+08	-7.09e+08	-1.77e+08
Point 3	2.25E+11	28,751.12	4.13e+08	-5.90e+08	-1.77e+08
Point 4	2.62e+11	26,769.59	3.58e+08	-5.06e+08	-1.47e+08
Point 5	3.00e+11	24,286.48	2.95e+08	-4.42e+08	-1.47e+08

The final two points amount to a different total energy value due to the fact that they are taken from the second leg of the transfer, shifting them to a different energy level.

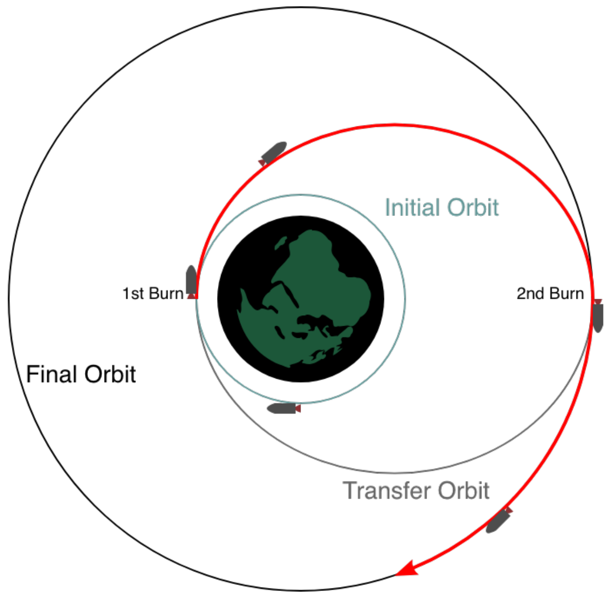

Fig. 1 Schematic of Hohmann transfer orbit diagram.[10]

Analytical mechanics is used in energy calculations. We begin with the simpler two-impulse Hohmann transfer with a case study on the Mars-Earth-Sun system, then the three-impulse bi-elliptic transfer, followed by the analysis of the JWST probes and Lagrange points. Eigenvalue Analysis is used in determining the stability of such points, as well as Astrodynamics Ephemerides and Angular Separation.

Hohmann Transfer

The Hohmann transfer is a two-impulse maneuver that transfers a spacecraft from a lower circular orbit (radius r1) to a higher circular orbit (radius r2). The first impulse (Velocity change $\Delta V1$) is applied to transfer the spacecraft from the lower circular orbit to the transfer ellipse. The second impulse brings it to the final orbit.

The initial conditions are as follows:

Table 3 Initial conditions of Hohmann Transfer

$r_1(m)$	1.46×10^{11}
$r_2(m)$	2.279×10^{11} (Mars)
$v_1(m/s)$	$\sim 32,700$
Phase Angle ϕ	$\sim 44.4°$
Transfer time	~ 259 days

The semi-major axis of the transfer ellipse A_{trans} is given by:

$$A_{\text{trans}} = \frac{r_1 + r_2}{2} \tag{2}$$

As it is the average of the two orbits, r_1 being initial and r_1 being final orbital radius. When transitioning from a circular orbit to an elliptical orbit, the velocity at the periapsis (the lowest point in the elliptical orbit) is given by:

$$V_1 = \sqrt{\frac{\mu}{r_1}} \tag{3}$$

Meanwhile, the initial velocity in the circular orbit is:

$$V_2 = \sqrt{\frac{\mu}{r_1}} \tag{4}$$

Therefore, the required change in velocity is:

$$\Delta V_1 = \sqrt{\mu(\frac{2}{r_1} - \frac{2}{r_1 + r_2})} - \sqrt{\frac{\mu}{r_1}} \tag{5}$$

The spacecraft then follows the elliptical transfer orbit from periapsis to apoapsis. At apoapsis, a second velocity change (ΔV_2) circularizes the orbit to r_2:

$$\Delta V_2 = \sqrt{\frac{\mu}{r_2}} - \sqrt{\mu(\frac{2}{r_2} - \frac{1}{A_{\text{trans}}})} \tag{6}$$

As a case study, we analyze the time window optimal for a probe launch with Mars. It will calculate the launch date for the trajectory of a spacecraft to intersect the orbit of Mars while minimizing flight time, using the Hohmann Transfer.

Following assumptions are made:

- Both Earth and Mars follow circular orbits around the Sun.
- The spacecraft only requires two velocity changes (at departure from Earth and at arrival to Mars).
- Ignoring other all celestial influences (e.g., the Moon, other planets).

$$\phi = \pi \left(1 - \frac{T_E}{T_M}\right) \tag{7}$$

Where:

- T_E is the orbital period of Earth around the Sun. T_M is the orbital period of Mars around the Sun. π represents the angular separation in radians between the planets.

For simplification:

- The average distance from Earth to the Sun is approximately 1 au (astronomical unit).
- The average distance from Mars to the Sun is approximately 1.524 au.

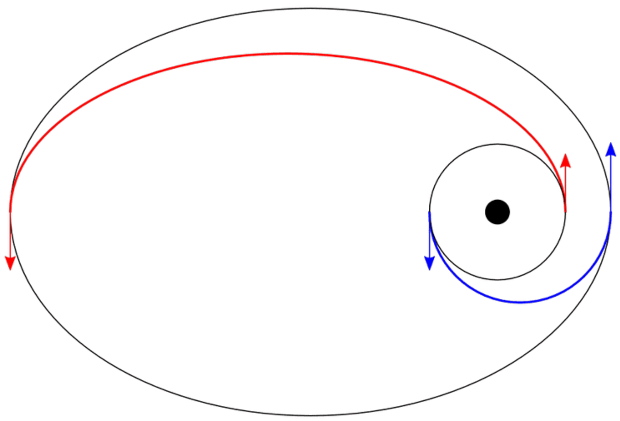

Fig. 2 Schematic of bi-elliptic transfer orbit diagram.[11]

Using Kepler's third law:

$$T \propto a^{3/2}$$

Where T is the orbital period and a is the semi-major axis. Thus, the ratio of Mars' orbital period to Earth's can be approximated by:

$$\frac{T_M}{T_E} \approx 1.88 \quad (8)$$

The synodic period can be calculated:

$$\frac{1}{T_s} = \left| \frac{1}{T_E} - \frac{1}{T_M} \right| = 780 \text{ d} \quad (9)$$

We can also obtain the intermediate orbits period and radius:

$$A_{\text{trans}} = \frac{R_1 + R_2}{2} = 1.762 \, \text{au} \quad (10)$$

$$T = 2\pi \sqrt{\frac{a^3}{\mu_\odot}} \approx 259 \, \text{d} \quad (11)$$

Where $\mu_\odot$ is the standard gravitational parameter of the Sun. The best alignment thus occurs when Mars is approximately 44 degrees (0.77 radians) ahead of Earth in their respective orbits, occuring every 2.14 years. The next launch window will occur in November 2025. The following table further elaborates on the data, calculating the angular difference of Earth and Mars in there orbits on monthly intervals, in radians. Each value is obtained by plugging in the value of time with the angular difference for each timestep:

Table 4 Positional difference between Earth and Mars any given month in the synodic period. This table shows, in radians, how much further Earth or Mars is in orbit, and how long it will take to reach another aligned position. First column denotes the amount of months since start of synodic period, the second column converts it to days, and the third, fourth, and fifth column show Earths, Mars, and their relative positions in radians, respectively.

Month	Days since start	Earth position (radians)	Mars position (radians)	Angular Difference (radians)
0	0	0	0	0
1	30	0.5161	0.2744	6.0415
2	60	1.0321	0.5488	5.7998
3	90	1.5482	0.8232	5.5581
4	120	2.0643	1.0976	5.3165
5	150	2.5804	1.372	5.0748
6	180	3.0964	1.6463	4.8331
7	210	3.6125	1.9207	4.5914
8	240	4.1286	2.1951	4.3497
9	270	4.6447	2.4695	4.108
10	300	5.1607	2.7439	3.8664
11	330	5.6768	3.0183	3.6247
12	360	6.1929	3.2927	3.383
13	390	6.7089	3.5671	3.1413
14	420	7.225	3.8415	2.8996
15	450	7.7411	4.1159	2.6579
16	480	8.2572	4.3902	2.4163
17	510	8.7732	4.6646	2.1746
18	540	9.2893	4.939	1.9329
19	570	9.8054	5.2134	1.6912
20	600	10.3215	5.4878	1.4495
21	630	10.8375	5.7622	1.2078
22	660	11.3536	6.0366	0.9662
23	690	11.8697	6.311	0.7245

Bi-elliptic transfers

The bi-elliptic transfer is a three-impulse maneuver used for large changes in orbital radius. The spacecraft is transferred from an initial orbit radius r_1 to a final orbit radius r_3 via an intermediate elliptical orbit with apoapsis radius r_2).

The initial conditions are as follows:

Table 5 Initial conditions of Bi0elliptic Transfer

$r_1(m)$	1.46×10^{11}
$r_2(m)$	2.279×10^{11} (Mars)
$v_1(m/s)$	$\sim 37,700$
Phase Angle ϕ	$\sim 100.26°$
Transfer time	~ 1564.86 days

An initial velocity change (ΔV_1) transfers the spacecraft from r1 to the intermediate elliptical orbit with semi-major axis $(r_1 + r_2)/2$, required velocity change being Delta v1. The spacecraft then follows the elliptical orbit from periapsis at r_1 to apoapsis at r_2. At r_2, a second velocity change (ΔV_2) transfers the spacecraft to a second elliptical orbit with semi-major axis A_{trans2}, required velocity change Delta v2. The spacecraft follows the second elliptical orbit from apoapsis at r_2 to periapsis at r_3. At r_3, a final velocity change (ΔV_3) circularizes the orbit:

$$\Delta V_3 = \sqrt{\frac{\mu}{r_3}} - \sqrt{\frac{2\mu}{r_3} - \frac{\mu}{A_{\text{trans2}}}} \tag{12}$$

The use of a third burn in the Bi-elliptic transfer introduces a higher energy reserve to complete the maneuver, meaning that it is more efficient only in some circumstances. The same applies to the two-impulse Hohmann transfer. Borderline orbital radius ratio can be calculated as follows.

As shown before, the initial velocity is:

Orbital Maneuver Comparison

$$V = \sqrt{\frac{\mu}{r}} \tag{13}$$

The speed after the first burn, at the perigee of the Hohmann ellipse, is therefore:

$$v_p = \sqrt{\mu(\frac{2}{r_1} - \frac{2}{r_1 + r_2})} \tag{14}$$

Speed before second burn at the apogee of the Hohmann ellipse v_a is the same value. Therefore, with the final orbital velocity, we can calculate that the total velocity change as:

$$\Delta v_{\text{Hohmann}} = (v_p - v_1) + (v_2 - v_a) \tag{15}$$

For the Bi-elliptic transfer, the first impulsive velocity change allows the spacecraft to enter the transfer ellipse:

$$\Delta v_1 = \sqrt{\mu(\frac{2}{r_1} - \frac{2}{r_1 + r_b})} \tag{16}$$

When finding the minimum Δv_2, we can take the limit of r_2 as it approaches positive infinity. At that point, Δv_2 approaches zero. Therefore the speed at r_2 before circularization is $\sqrt{\frac{2\mu}{r^2}}$, and we can calculate the final maneuver as well as the total Δv:

$$\Delta v_3 = \sqrt{\frac{\mu}{r_2}} - \sqrt{\mu(\frac{2}{r_2} - \frac{2}{r_b + r_2})} \tag{17}$$

$$\begin{aligned} \Delta v_{\text{bi-elliptic}} = {} & \sqrt{\mu(\frac{2}{r_1} - \frac{2}{r_1 + r_b})} - \sqrt{\frac{\mu}{r_1}} + \sqrt{\mu(\frac{2}{r_b} - \frac{2}{r_2 + r_b})} \\ & - \sqrt{\mu(\frac{2}{r_b} - \frac{2}{r_1 + r_b})} + \sqrt{\frac{\mu}{r_2}} - \sqrt{\mu(\frac{2}{r_2} - \frac{2}{r_2 + r_b})} \end{aligned} \tag{18}$$

If we normalize both equations with initial velocity as v_c, ratio between radii as R, then we can organize both expressions:

$$\begin{aligned} \frac{\Delta v_{\text{Bi-elliptic}}}{v_c} = {} & \left(\sqrt{2 - \frac{2}{1+\beta}} - 1\right) \\ & + \left(\sqrt{\frac{2}{\beta} - \frac{2}{\beta(\beta+R)}} - \sqrt{\frac{2}{\beta} - \frac{2}{\beta(1+\beta)}}\right) \\ & + \left(\frac{1}{\sqrt{R}} - \sqrt{\frac{2}{R} - \frac{2}{R(\beta+R)}}\right) \end{aligned} \tag{19}$$

$$\frac{\Delta v_{\text{Hohmann}}}{v_c} = \left(\sqrt{2 - \frac{2}{1+R}} - 1\right) + \left(\frac{1}{\sqrt{R}} - \sqrt{\frac{2}{R} - \frac{2}{R(1+R)}}\right) \tag{20}$$

Solving the following equation numerically yields the passing point of radii ratio:

$$\left(\sqrt{2} - 1\right) + \frac{1}{\sqrt{R}} - \sqrt{\frac{2}{R}} < \sqrt{\frac{2R}{1+R}} - 1 + \frac{1}{\sqrt{R}} - \sqrt{\frac{2}{R(1+R)}} \tag{21}$$

R is around 11.94. Thus, the limit to the effectiveness of the Hohmann transfer is up to a final orbit 11.94 times the radius of the initial.

Lagrange Points

Lagrange points were introduced through the restricted three-body problem. The restricted three-body problem considers two massive bodies, m_1 and m_2, in circular orbits around their common center of mass, and a third body of negligible mass m_3 influenced by the gravitational attraction of m_1 and m_2. Compared to the three-body problem, it essentially has one less

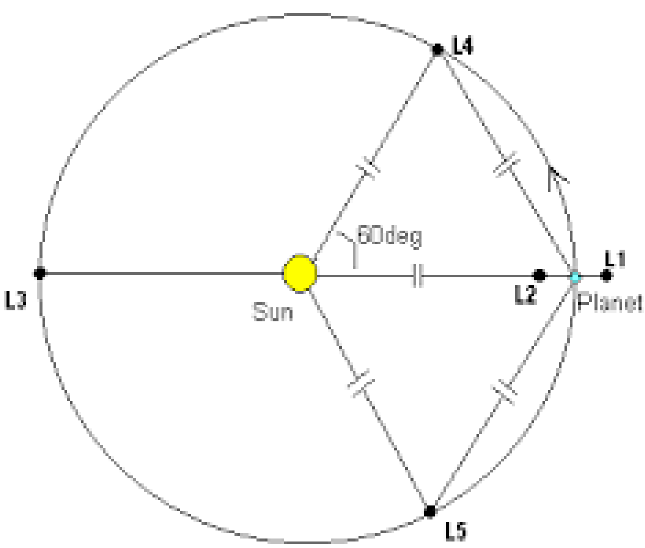

Fig. 3 Schematic of Lagrange points diagram.[12]

massive variable and focuses on the trajectory of the massless object. The positions of m_1 and m_2 are fixed in a rotating reference frame where the x-axis passes through both bodies, and the origin is the center of mass. In the rotating reference frame, the equations of motion for m_3 are given by:

$$\ddot{x} - 2\dot{y} = \Omega_x \tag{22}$$

$$\ddot{y} + 2\dot{x} = \Omega_y \tag{23}$$

where (x, y) is the effective potential energy. Lagrange points are the positions where the net force on m_3 is zero in the rotating frame. Therefore, at Lagrange points the following is true:

(24)

$$\Omega_y = \frac{\partial \Omega}{\partial y} = 0 \tag{25}$$

The solutions for x and y are the positions of the corresponding Lagrange points. We define μ as the mass ratio in the circular restricted three-body problem, where its value is between 0 and 1:

$$\mu = \frac{m_2}{m_1 + m_2} \tag{26}$$

The L1 point lies on the line connecting m_1 and m_2 between them. With L1 at x = R - r, where r is the distance from m_2 to L1 and R is defined as the orbital radius of the secondary body:

$$R - r - \frac{(1-\mu)(R - r + \mu)}{r_1^3} - \frac{\mu(R - r - 1 + \mu)}{r_2^3} = 0 \tag{27}$$

Where r_1 is the distance between m_3 and m_1 and r_2 is the distance between m_3 and m_2. For small r, this can be solved for the position of L1. The L2 point lies on the line connecting m_1 and m_2 beyond m_2. With L2 at x = R + r:

$$R + r - \frac{(1-\mu)(R + r + \mu)}{r_1^3} - \frac{\mu(R + r - 1 + \mu)}{r_2^3} = 0 \tag{28}$$

The L3 point lies on the line connecting m_1 and m_2 beyond m1. With L3 at $x = -r$:

$$-r - \frac{(1-\mu)(-r + \mu)}{r_1^3} - \frac{\mu(-r - 1 + \mu)}{r_2^3} = 0 \tag{29}$$

The L4 and L5 points form equilateral triangles with m_1 and m_2. For L4, the coordinates are $(\frac{1}{2} - \mu)R, (\frac{\sqrt{3}}{2})$

$$\Omega_x = \frac{1}{2} - \mu - \frac{(1-\mu)(\frac{1}{2} - \mu)}{R_3} - \frac{\mu R_3}{2} = 0 \tag{30}$$

$$\Omega_y = \frac{\sqrt{3}}{2} - (1-\mu)\frac{\sqrt{3}}{2R_3} - \frac{\mu\sqrt{3}R_3}{2} = 0 \tag{31}$$

Stability Analysis

To analyze the stability, this paper linearizes the equations of motion around the Lagrange points, thus:

$$x = x_0 + \delta x \tag{32}$$

$$y = y_0 + \delta y \tag{33}$$

When substituting into equations of motion, the following can be obtained:

$$\ddot{\delta} x - 2\dot{\delta} y = \Omega_{xx}\delta x + \Omega_{xy}\delta y \tag{34}$$

The following section elaborates on the evaluation and analysis of eigenvalues. In matrix form, L1 to L3 can be expressed as:

$$A = \begin{bmatrix} 0 & 0 & 1 & 0 \\ 0 & 0 & 0 & 1 \\ \Omega_{xx} & \Omega_{xy} & 0 & 2 \\ \Omega_{xy} & \Omega_{yy} & -2 & 0 \end{bmatrix}_{(x_0,0)} \tag{35}$$

At collinear points (L1, L2, L3), y = 0 by symmetry yields:

$$\Omega_{xy} = 0 \tag{36}$$

and

$$\Omega_{xx} \neq \Omega_{yy} \tag{37}$$

Simplifying the determinant of this matrix can give a solvable bi-quadratic equation:

$$\lambda^4 + (4 - a - b)\lambda^2 + ab = 0 \tag{38}$$

Solving this characteristic equation yields eigenvalues λ. The stability of the Lagrange points is determined by the real parts of the eigenvalues. If all real parts of λ are negative, the point is stable. If any real part of λ is positive, the point is unstable. When plugging in the previous equation to the quadratic formula, the eigenvalue can be simplified:

$$\lambda^2 = \frac{-(4-a-b) \pm \sqrt{(4-a-b)^2 - 4ab}}{2} \tag{39}$$

For L1, L2, and L3, they generally have eigenvalues with positive real parts, indicating instability. Small perturbations grow over time, causing the spacecraft to drift away.

The matrix for L4 and L5 is slightly different, with

$$\Omega_{xy} = 0 \tag{40}$$

and

$$\Omega_{xx} = \Omega_{yy} \tag{41}$$

Expressed as

$$A = \begin{bmatrix} 0 & 0 & 1 & 0 \\ 0 & 0 & 0 & 1 \\ \Omega_{xx} & 0 & 0 & 2 \\ 0 & \Omega_{xx} & -2 & 0 \end{bmatrix} \tag{42}$$

The characteristic equation is

$$\lambda^4 + (4 - 2\Omega_{xx})\lambda^2 + \Omega_{xx}^2 = 0 \tag{43}$$

For L4 and L5, the eigenvalues are purely imaginary under the mass ratio of the Earth-Sun system, indicating neutral stability. Small perturbations neither grow nor decay, resulting in stable oscillatory motion around the points. However, when the mass ratio exceeds the Routh stability criterion, none of the Lagrange Points are stable balances.

Table 6 Lagrange Point eigenvalue analysis

Point	Eigenvalues	Stability
L1	$\pm\lambda, \pm i\omega$	Unstable
L2	$\pm\lambda, \pm i\omega$	Unstable
L3	$\pm\lambda, \pm i\omega$	Unstable
L4	$\pm i\omega_1, \pm i\omega_2$	Stable if $\mu < 0.0385$
L5	$\pm i\omega_1, \pm i\omega_2$	Stable if $\mu < 0.0385$

Thus, the stability analysis shows that generally L1, L2, and L3 are unstable, while L4 and L5 are stable.

JWST Case Study

In this section we delve deep into the HALO orbit taken by the JWST(James Webb Space Telescope) probe.

In the restricted three body problem, we consider two large bodies (e.g., Sun and Earth) and a third negligible-mass object (JWST). The five Lagrange points are in equilibrium in the rotating frame. Of these, L_2 lies outside Earths orbit, along the SunEarth axis. The motion of JWST in this rotating frame is governed by the equations:

$$\ddot{x} - 2\dot{y} = \frac{\partial \Omega}{\partial x} \tag{44}$$

$$\ddot{y} + 2\dot{x} = \frac{\partial \Omega}{\partial y} \tag{45}$$

$$\ddot{z} = \frac{\partial \Omega}{\partial z} \tag{46}$$

where (x,y,z) is the effective potential:

$$\Omega = \frac{1}{2}(x^2 + y^2) + \frac{1-\mu}{r_1} + \frac{\mu}{r_2} \tag{47}$$

The HALO orbit is in essence periodic solutions to the restricted three-body problem near collinear Lagrange Points. In an ideal situation, the orbit around L2 would not require any maintenance. Even when accounting for perturbations, the thrust required is many orders of magnitudes less than if the spacecraft was positioned at L2 directly. The aim is to minimize the unstable eigenvalue mode. Let the eigenvalue λ represent the unstable mode:

$$x(t) = Ae^{\lambda t} \tag{48}$$

A small deviation grows exponentially. By choosing an orbit along the center manifold and away from the unstable direction, the spacecraft avoids this exponential drift, and only small corrections are needed to stay close to the HALO. Mathematically, for small perturbation x along the unstable direction,

$$\delta x(t) \approx \delta x_0 e^{\lambda t} \tag{49}$$

Where δx_0 is the magnitude of initial deviation along the unstable eigenvector and $\delta x(t)$ is that value after a period of time. Controlling $\Delta v \sim \lambda x(t)$ to align with the periodic orbit suppresses long term drift.

Results

The results of the simulation prove and summarize how multi-impulse orbital transfers act in the specific way they do. As shown in Fig. 1 and Fig. 2, orbital rendezvous and transfer between orbits following the bi-elliptic transfer grants more efficiency when the orbital ratios reach a certain point. The coding will be in the appendix section. The total potential energy, as simulated below, implies that when catching up with a body moving faster, a spacecraft should decrease its orbits axis

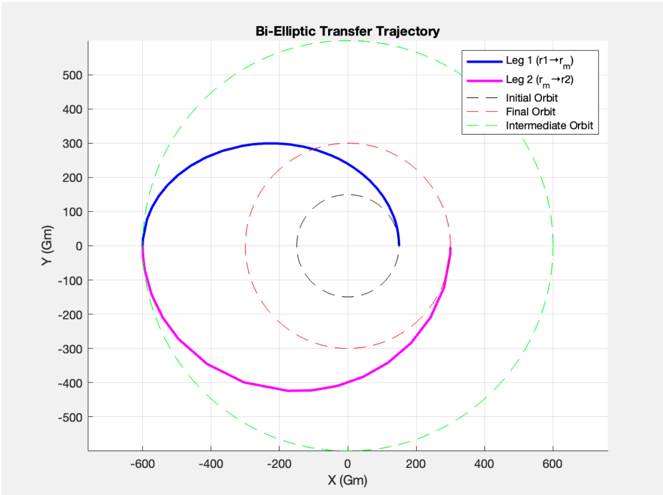

Fig. 4 Plot of bi-elliptic transfer. The main body is set at the origin of the graph, and we plot the transfer trajectory from initial (Blue) to final (Red) orbit. Three impulsive velocity changes are positioned on the intersection of the trajectory with the orbits.

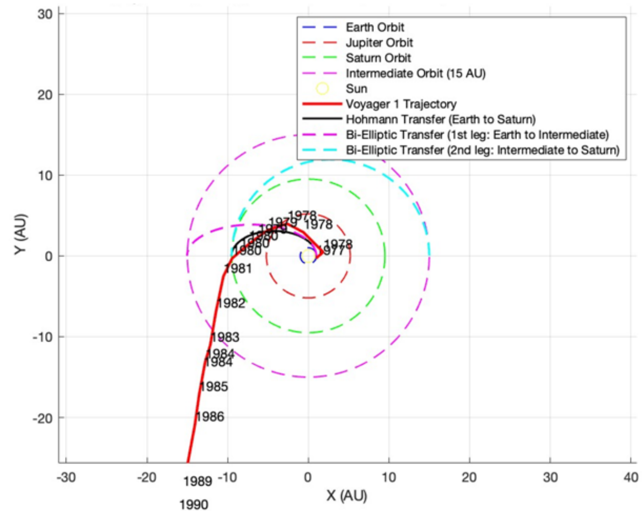

Fig. 6 Comparison of Voyager 1 Trajectory with that of Hohmann and bi-elliptic transfers to Saturn. The ephemeris data was used to determine Voyager 1s position, taking into account the slingshot effect used. Hybrid transfer provides it with more terminal velocity and greater fuel efficiency.

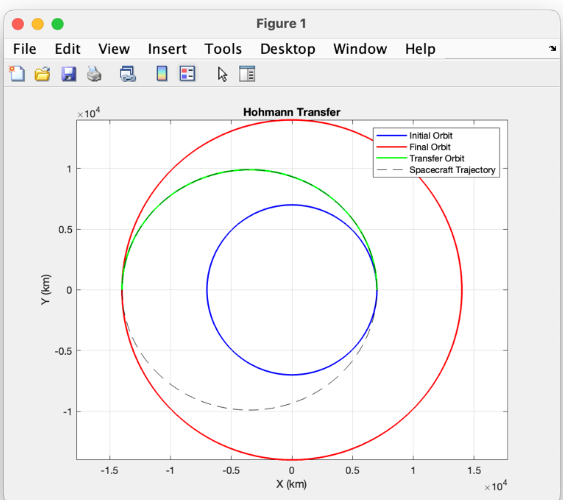

Fig. 5 Plot of Hohmann transfer. The main body is set at the origin of the graph, and we plot the transfer trajectory from initial (Blue) to final (Red) orbit. The required velocity changes occur at the periapsis and apoapsis of the initial and transfer orbits, respectively.

for a smaller orbit. The conversion of energy grants a deltaV for transferring.

Through further comparison, we conclude that Bi-elliptic transfers are more efficient when the ratio between initial and destination orbital radii exceeds 11.94 times. Due to the extra burn and adoption of the intermediate ellipses, the Bi-elliptic transfer is optimal for larger scale maneuvers. The tradeoff for a smaller delta v requirement is enlongated mission duration, making the spacecraft trajectory suscepticle to perturbations. A tighter launch window also needs be taken into account for optimal alignment.

This study further compares the two transfers with the integration of the slingshot effect. In the case study of the Voyager 1 probe, it is found that the integrated orbit proves to be the most energy efficient, utilizing the suns gravity well to accelerated towards outside of the solar system. Figure 3 below denotes the trajectory of the three different approaches.

In the stability analysis, this research finds minor perturbations have little direct effect on the orbit. Orbital decay can be seen as the major force that leads to instability, where the gradual force slowly increases the eccentricity of the orbit. As denoted by Fig. 4 below, the effect of decay expands slowly at first and then falls into increasing chaos. The collinear L1, L2, and L3 points require continuous or periodic station-keeping, as small perturbations can grow exponentially due to the local saddle-point dynamics. Though the required delta v is relatively low, the high precision and frequency of control maneuvers demand robust navigation and propulsion systems, as exemplified by missions such as JWST. This implies that any orbit taken at L1, L2, and L3 requires constant maintenance while those at L4 and L5 are more stable.

The plots below are created in relation to the results of the JWST analysis. With further comparison to NASA ephemeral data parameters, the trajectory plotted is extremely close to observed results [13]. The HALO orbit adapted requires minimal energy reserve to maintain. By adopting station-keeping burns

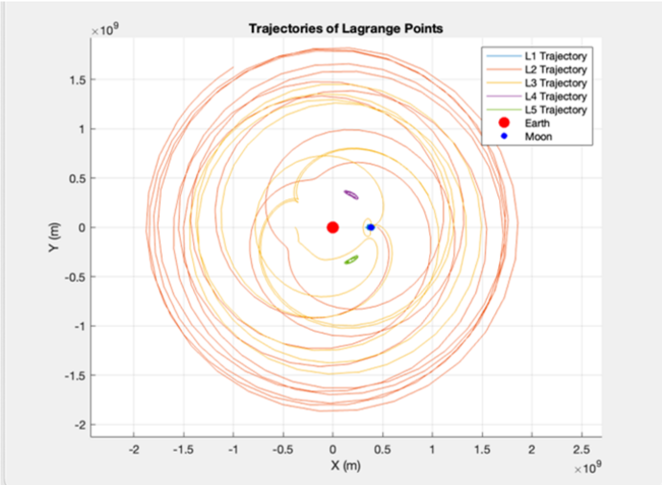

Fig. 7 Plot of Lagrange Points. The plot shows the inherent instability of L1, L2, and L3, as they spiral outward quickly when the unstable balance is slightly broken by a simulated perturbation. L4 and L5 stay relatively stable.

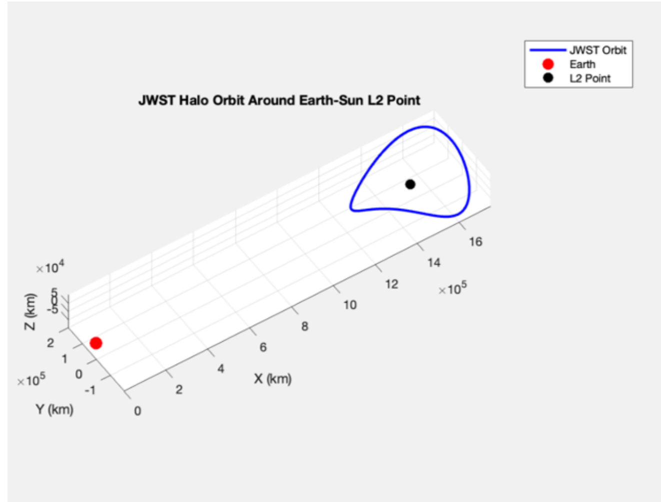

Fig. 9 The trajectory of the HALO orbit in space relative to Earth. The saddle-like shape allows for fuel-efficient station keeping.

approximately every three weeks, JWST stays locked around the unstable equilibrium, while its relative position to the Earth-Sun system remains similar. This allows for consistent observation, under the premise of the restricted three-body problem.

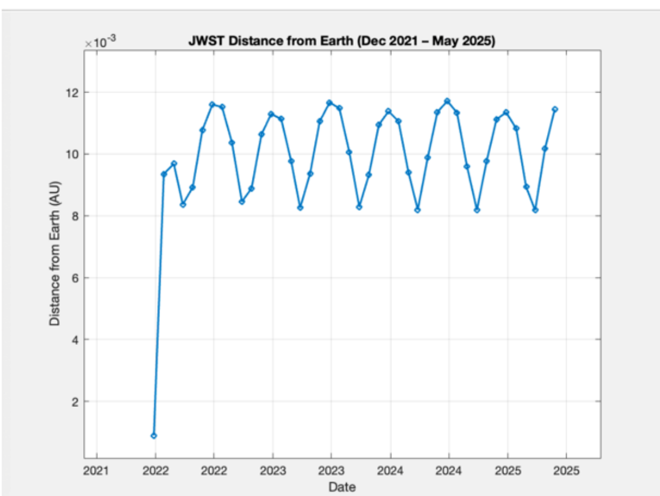

Fig. 8 JWSTs stable orbit and oscillating distance from Earth. The L2 HALO orbit keeps the distance from exceeding a minimal and maximal distance.

This study further examines the gravitational field strength any distance away from the sun in the solar system. The result is in Figure 5 below. The suns gravitational potential is graphed as the red line, while the intersections are where the planets strength overcomes that. The total gravitational field strength further denotes the net force acting on a spacecraft. When accounting for missions that approach or land on a planet, the results in this graph where the black line shifts away from the red line are the orbital radii to aim for in a mission. The following table highlights these points.

Table 7 Gravity well thresholds. The left column denotes which planets gravitational field a spacecraft enters at corresponding orbital radii. The right column states different values of distances away from the sun, where the gravitational pull of a planet overcomes that of the sun.

Intersection	**Orbital radii (from the edge of the sun, in au)**
Mercury	0.387 738
Venus	0.7077 01
Earth	0.986 266
Mars	1.503 76
Jupiter	4.098 38
Saturn	8.070 62
Uranus	17.999 3
Neptune	28.018 7

Discussion

The current analysis assumes an ideal two-body problem with Earth as the primary focus. However, real-world scenarios involve perturbative forces such as solar radiation pressure, gravitational influences from other celestial bodies, atmospheric drag (for LEO), and the oblateness of the Earth. The simulations calculated have been compared to official ephemeris data and energy reserve. When not accounting for perturbations, this study tends to underestimate required fuel consumption and

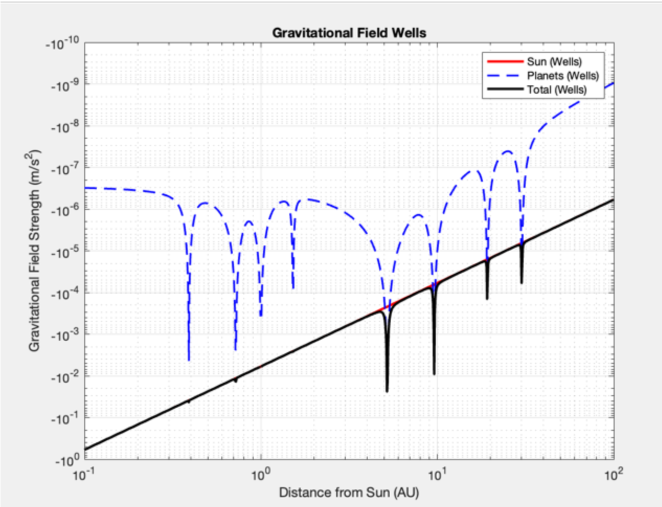

Fig. 10 Gravitational field well plot. The blue line denotes the planets gravitational pulls at corresponding distances from the sun, the red line is the suns gravitational pull, and the black line is the net pull on an object. Scale is logged for visual purposes.

corrective velocity changes. The transfer schedule remains consistent with the database. Future work could involve integrating these perturbations into the simulations to assess their impact on the efficiency and stability of Hohmann and Bi-elliptic transfers.

The total delta-v is a crucial parameter for mission planning, yet fuel restraints and such factors can limit the possibility of maneuvers. Investigating hybrid transfer strategies that combine aspects of Hohmann, bi-elliptic, and low-thrust transfers could lead to more efficient and versatile mission plans. While this study focuses on Earth-centered orbits, the principles and findings can still be extended to interplanetary missions. Analyzing transfers between planets, where the differences in gravitational fields and the presence of additional celestial bodies play significant roles, could open up new insights into interplanetary travel. The different variables and atmospheric differences will need to be addressed.

This study assumes the use of traditional chemical propulsion for the orbital transfers. Future research could explore the implications of using advanced propulsion systems such as ion thrusters, electric propulsion, or solar sails. All of these offer continuous low thrust, calling for new transfer methods that account for the lack of impulsive changes. Developing and refining simulation tools that can model these transfer methods in various scenarios are thus crucial for mission design.

In the stability analysis, the trajectory of Lagrange points can be seen to become unstable very drastically. This implies that maneuvers and fuel needs to be spent when parking into any Lagrange point. However, the use of HALO orbits can accommodate the circular motion in many scenarios. When incorporating perturbations outside of the system, this study implies that intricate balancing can be crucial for future missions. This universal interpretation allows for spacecraft to dock in such points in not just the Earth-moon system, but in any two-body system.

The coding basis of this study can also be applied to further research on any and all systems. As has been studied upon in various launches, the energy required to reach the gravitational balancing point can be used for various purposes. Any flyby or landing will require the use of such calculations. Further implications include further optimization of maneuvers and utilization of hybrid transfers with innovative propulsion methods to achieve maximum efficiency.

Conclusion

This study successfully confirmed theoretical predictions regarding the positions and stability of the Lagrange points in the Earth-Moon system. The stability analysis highlighted the inherent instability of L1, L2, and L3, while L4 and L5 were found to be neutrally stable under specific conditions. The bi-elliptic transfer analysis demonstrated its potential efficiency for specific orbital maneuvers, particularly for large changes in orbital radius. These allow for the complex trajectory planning used in almost all recent missions. Understanding the dynamics and stability of these points is crucial for mission design, especially for long-term station-keeping, deep space missions, and exploration strategies involving stable orbits around L4 and L5. The implications of these findings extend beyond the Earth-Moon system. The methods and results can be generalized to other three-body systems, such as the Sun-Earth or Sun-Jupiter systems, enabling more efficient mission designs and trajectory optimizations in various contexts. Future steps include refining the perturbation models to account for more complex forces to optimize transfer strategy.

References

1 A. Einstein, *Relativity: The Special and General Theory*, 2021.

2 N. Copernicus, E. Rosen and G. J. Rhaticus, *Three Copernican Treatises: The Commentariolus of Copernicus, the Letter against Werner, the Narratio Prima of Rheticus*, 1959.

3 J. Kepler, E. J. Aiton, A. M. Duncan and J. V. Field, *The Harmony of the World*, 1997.

4 M. Wilson, *1997ESASP.403..341W Page 341*, `https://adsabs.harvard.edu/full/1997ESASP.403..341W`, 2024, Accessed 2024.

5 W. Hohmann, *Die Erreichbarkeit Der Himmelskrper*, 2019.

6 R. F. Hoelker and R. Silber, *The Bi-Elliptical Transfer between Co-Planar Circular Orbits*, 1961.

7 J. L. Lagrange, *Mcanique Analytique*, 1811.

8 Ahmed, *Fifty Years of Halo Orbits*, https://ui.adsabs.harvard.edu/abs/2023DDA....5420403D/abstract, 2023.

9 L. F. Shampine and M. W. Reichelt, *The MATLAB ODE Suite*, 1997.

10 B. Weber, *Hohmann Transfer Orbital Mechanics & Astrodynamics*, https://orbital-mechanics.space/orbital-maneuvers/hohmann-transfer.html, Accessed 2024.

11 D. Lane, *Computational Hohmann Transfer*, https://physicsforums.com/threads/computational-hohmann-transfer-on-maplesoft.946891/, 2018, Accessed 2024.

12 *Lagrange Points*, https://www.spaceacademy.net.au/library/notes/lagrangp.htm, 2011, Accessed 2024.

13 R. Park, *Horizons System*, https://ssd.jpl.nasa.gov/horizons/app.html#/, Accessed 2024.

Appendix

The code and basic logic to the plots in this study can be found via this link.
https://miniature-space-chainsaw-v6rx9759xpq5hwp65.github.dev/